SUBJECT: **Matching SPIRE - HOB Decentre and tilt amplitudes to the Photometer pupil alignment budget**

PREPARED BY: **A G Richards**

KEYWORDS: **alignment budget, tilts, displacements**

COMMENTS: **General relationships between SPIRE boresight displacements and tilts and the random decentres and tilts likely at the SPIRE - HOB interface are derived. These permit accurate estimation of the amplitudes allowed for the decentres and tilts**

DISTRIBUTION:

B. Swinyard	(RAL)	
M Caldwell	(RAL)	
M Ferlet	(RAL)	
K.Dohlen	(LAM)	
Project Office	(RAL)	

Contents

1. INTRODUCTION

The optical error budgets for SPIRE include the following error budget tree (figure 1-1) relevant to the effects of misalignments and tilts on the overall SPIRE Photometer Pupil alignment with the telescope pupil at M2. The pupil misalignment ΔR is quoted as a percentage of the Telescope pupil radius R. A total of 12.3% has been budgeted, broken down as shown.

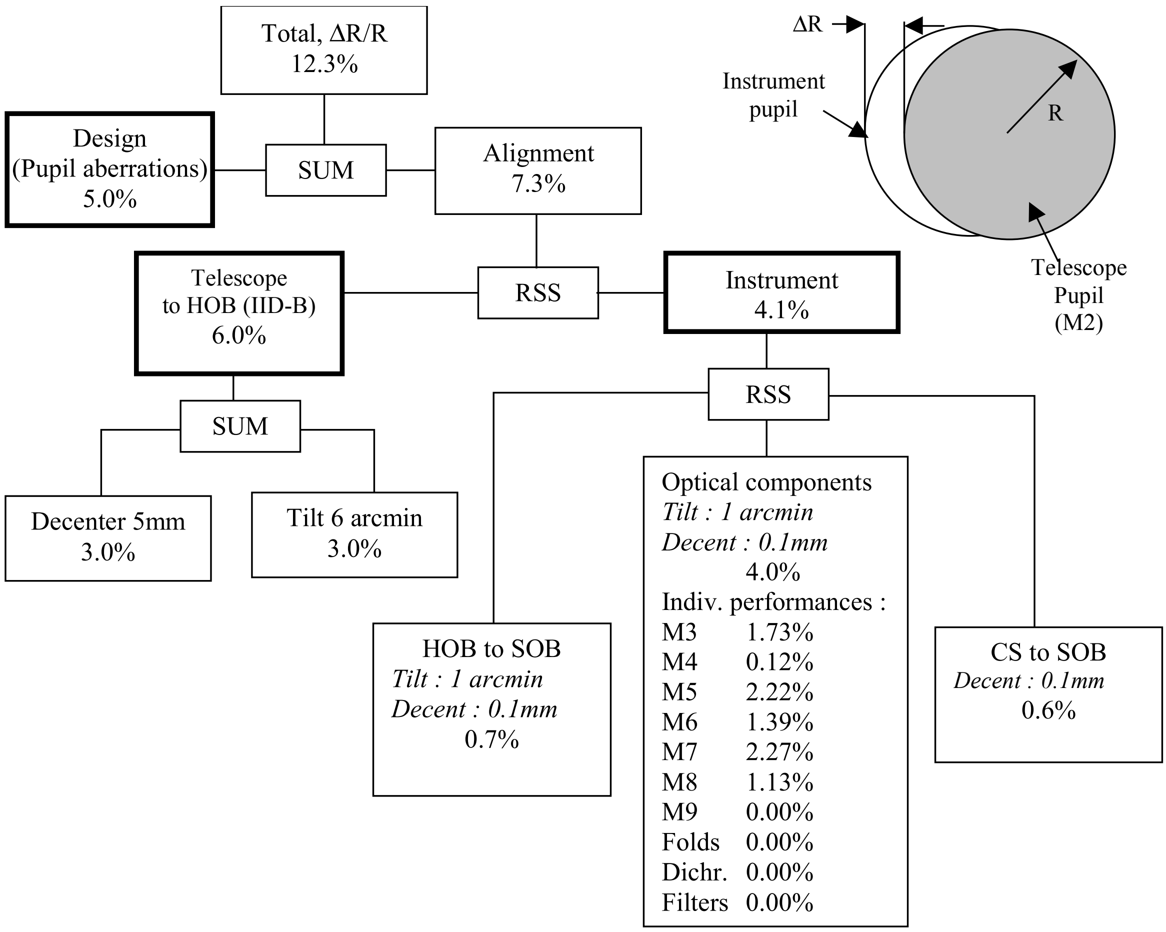

Figure 1-1 Photometer pupil alignment error budget

The box on the left marked "Telescope to HOB" not only sums the contributions from all the tilts and displacements due to mispositioning of the Hershel Optical Bench (HOB) relative to the telescope, but must also include the effects due to mispositioning of SPIRE on the HOB. This 6% total is root-sum-squared with a total instrument contribution of 4.1%. The instrument total contains a contribution of 0.7% labelled "HOB to SOB", but this is actually intended as a contribution due to misalignment of the optical reference surface on the SOB relative to the SPIRE boresight, leading to misalignment of SPIRE on the HOB.

So a total of 6% pupil alignment error has been allotted to the effects of mispositioning SPIRE on the HOB (via displacements and tilts from the optimum position) and resulting from mispositioning the HOB relative to the telescope optical axis and focus.

This note summarises the work carried out to try and establish general relationships between SPIRE boresight displacement and tilt and the 3-axes random decentres and tilts likely at both the SPIRE – HOB and HOB – Telescope interfaces. Once established, they would permit accurate estimation of the amplitudes allowed for the random decentres and tilts for each axis whilst ensuring, with reasonably high probability, that their total contribution remains less than or equal to the budgeted 6%.

2. EFFECT OF MISALIGNMENTS ON THE SPIRE INSTRUMENTS' BORESIGHT.

The effects of internal (mounting of SPIRE to the Herschel optical bench, HOB) and external (alignment of the HOB to the telescope) misalignments on the SPIRE photometer and spectrometer are to

- Modify each instrument's boresight direction,
- Laterally displace the boresight vector for each instrument from pointing towards the centre of M2,
- Displace each instrument from its position of best focus relative to the telescope.

3. SOURCES OF MISALIGNMENT

The likely major sources are listed as follows:

- 'Rocking' of SPIRE due to non-flatness of the Herschel optical bench (HOB) causing displacement of two feet from their designed positions – two angles required.
- Rotation of SPIRE in the plane of the HOB – one angle required.
- Displacement of SPIRE along 3 orthogonal axes from its optimum position on the HOB – 3 displacements needed.
- Rotation of the HOB about three axis – 3 angles needed.
- Displacement of the HOB along 3 orthogonal axes from its optimum position – 3 displacements needed.

4. GEOMETRY USED

In what follows, the photometer geometry will be focussed on to illustrate in detail the movement of the alignment of SPIRE due to positioning and tilt errors. The treatment for the spectrometer is essentially the same as is presented here.

For simplicity, I have reverted to using a co-ordinate system where the HOB is nominally at Z=0 in a system with +Z along the telescope axis, +X in the fold plane of the SPIRE photometer, +Y 90 degrees to the fold plane, with SPIRE in its optimum position. In this system (illustrated, for the photometer, in figure 4-1), SPIRE is perfectly located when the photometer boresight intersects the centre of M2, which is Zbore mm away along the axis, at an angle α to the axis. The azimuth angle β of the SPIRE photometer's fold plane is then equal to zero. The analysis for the spectrometer would utilise a different value for α and a non-zero value for β, together with a different location on M3 for the boresight vector (see table (8-1) for the main parameters defining the boresight geometry for both instruments).

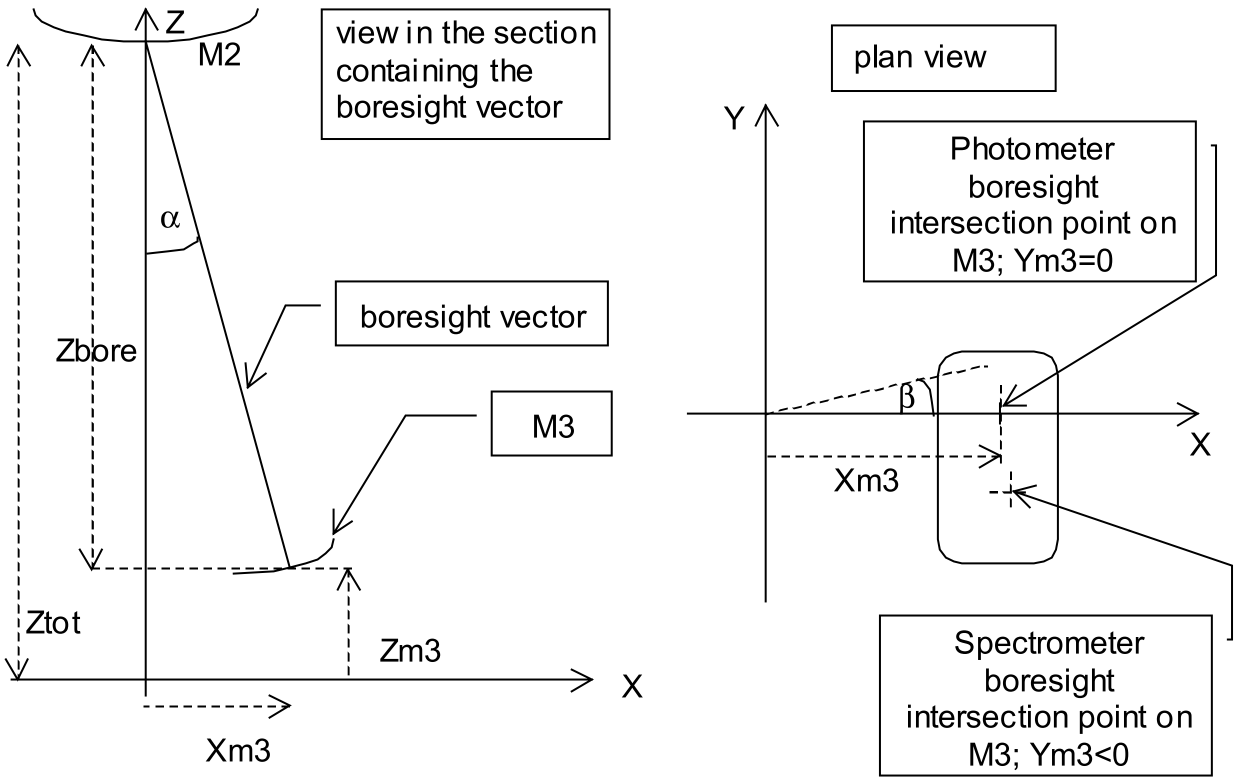

Figure 4-1 Boresight geometry

Here and in what follows, the 'boresight vector' follows the photometer's gut ray so the co-ordinates shown in figure 4-1 are of the gut ray intersection point with M3. The boresight vector is treated as a physical entity attached to M3 at the appropriate point, making the appropriate angle. This vector then partakes in all the gyrations and movements that M3 is subjected to, caused by the various tilt misalignments and de-centres that SPIRE (and hence M3) experiences. As a result, the instrument's boresight vector will be re-pointed in direction **(αnew,βnew)** and its foot, attached to M3, will be offset from its 'new' optimum boresight position by various amounts measured along all 3 axes. These offsets can be expressed (see figure 4-2) as a defocus (movement parallel to the direction of the 'new' boresight vector) and as lateral shifts parallel to the primed axes (X', Y') that are located in and at 90 degrees to the 'new' fold plane (which is now at azimuth **βnew**)

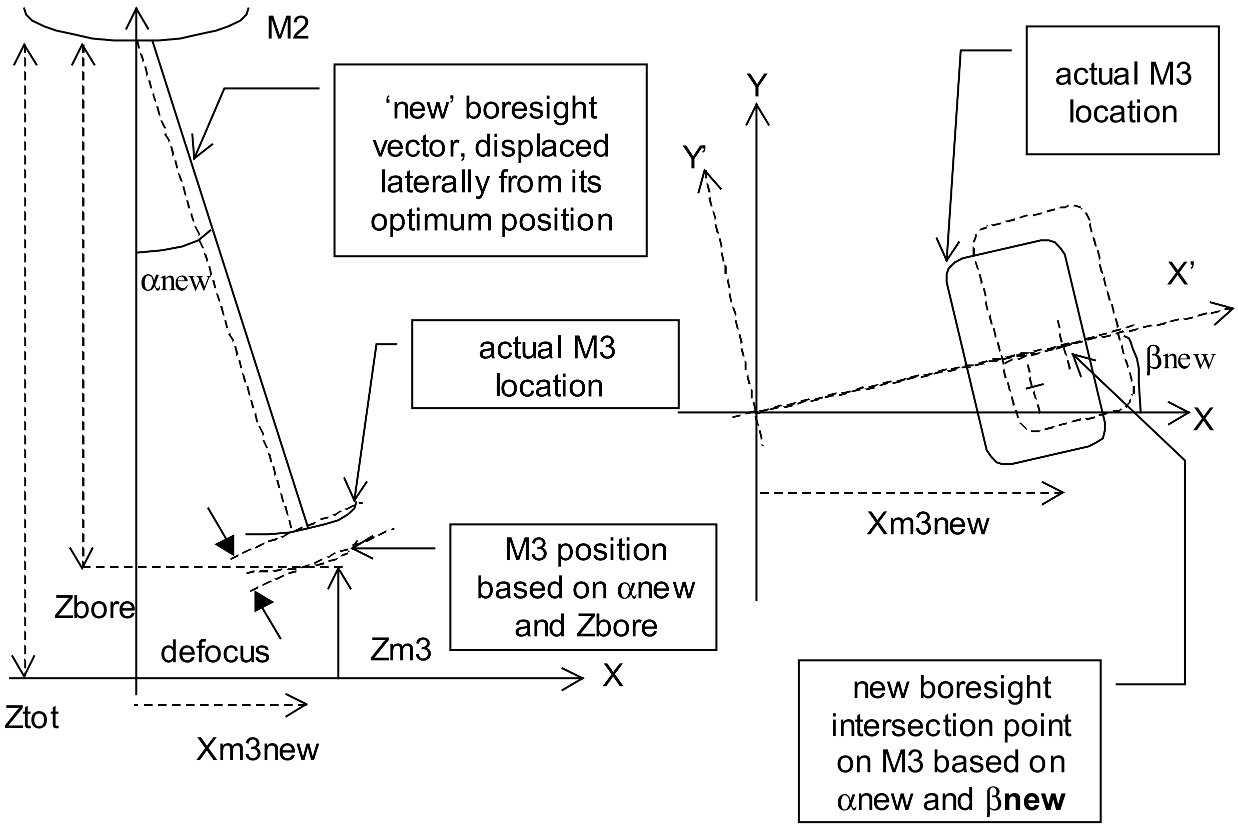

Figure 4-2 Geometry of M3 and 'new' boresight after tilts and de-centres of SPIRE and the HOB

5. MODELLING SPIRE TILTS DUE TO MOUNTING FEET DISPLACEMENTS

Figure 5-1 shows schematically the geometry of the SPIRE support system. Essentially, there is one inner foot, F1, which can act as a hinge, and two outer feet that may have different non-zero displacements normal to the HOB, as shown. These outer feet are symmetrically placed on either side of the photometer fold plane. The differential Z-displacements of the two outermost feet result in angular motions θ and ϕ about the two indicated axes. The subsequent rotations of SPIRE are then as a rigid body rotated about the hinge at F1. The location of F1 (XF, YF, ZF) is given relative to the same origin as is the optimum location of the boresight vector where its intersects M3, (Xm3, Ym3, Zm3). A third rotation δ about the nominal Z direction completes the triumvirate of tilts.

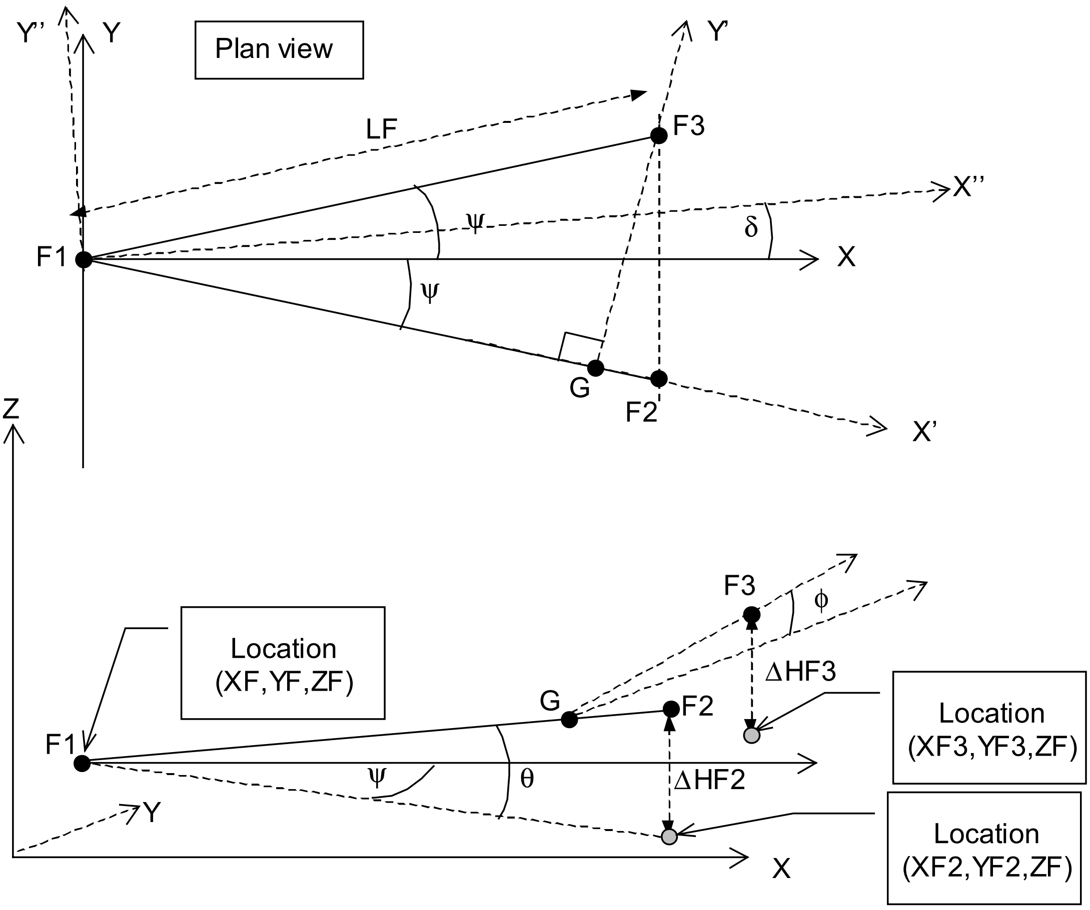

Figure 5-1

6. MODELLING HOB TILTS AND DISPLACEMENTS

The three HOB tilts (**ν,μ,λ**) are assumed to take place about a point on the telescope axis where it meets the HOB. Subsequent shifts of the HOB along all 3 axes, (δXhob, δYhob, δZhob) complete the effects of displacement of the HOB from its optimum location. All tilts and displacements of the HOB from its nominal position feed through as tilts and displacements of SPIRE.

7. COMBINING ALL THE TILTS AND DISPLACEMENTS

7.1. Effect on the boresight vector

Since all angular tilts will be small, the small-angle approximations sin(x)=x and cos(x)=1 will be used and terms involving products of angles will be neglected compared to terms linear in small angles. The full approximate expression for the transformation of a boresight vector (-sin(α)cos(β**)**, sin(α)sin(β**)**, cos(α)) is then given by

$$\begin{bmatrix}1&0&0&0\\0&1&0&0\\0&0&1&\lambda\\0&0&-\lambda&1\end{bmatrix}\cdot\begin{bmatrix}1&0&0&0\\0&1&0&-\mu\\0&0&1&0\\0&\mu&0&1\end{bmatrix}\cdot\begin{bmatrix}1&0&0&0\\0&1&\nu&0\\0&-\nu&1&0\\0&0&0&1\end{bmatrix}\cdot\begin{bmatrix}1&0&0&0\\0&1&\delta&0\\0&-\delta&1&0\\0&0&0&1\end{bmatrix}\cdot\begin{bmatrix}1&0&0&0\\0&\cos(\psi)&\sin(\psi)&0\\0&-\sin(\psi)&\cos(\psi)&0\\0&0&0&1\end{bmatrix}\cdot\begin{bmatrix}1&0&0&0\\0&1&0&-\theta\\0&0&1&0\\0&\theta&0&1\end{bmatrix}\cdot\begin{bmatrix}1&0&0&0\\0&1&0&0\\0&0&1&\phi\\0&0&-\phi&1\end{bmatrix}\cdot\begin{bmatrix}1&0&0&0\\0&\cos(\psi)&-\sin(\psi)&0\\0&\sin(\psi)&\cos(\psi)&0\\0&0&0&1\end{bmatrix}\cdot\begin{bmatrix}0\\-\sin(\alpha)\cdot\cos(\beta)\\\sin(\alpha)\cdot\sin(\beta)\\\cos(\alpha)\end{bmatrix}$$

Which can be condensed to

$$\begin{bmatrix} 1 & 0 & 0 & 0 \\ 0 & 1 & \nu+\delta & \phi\cdot\sin(\psi)-\theta\cdot\cos(\psi)-\mu \\ 0 & -\nu-\delta & 1 & \phi\cdot\cos(\psi)+\theta\cdot\sin(\psi)+\lambda \\ 0 & \mu+\theta\cdot\cos(\psi)-\phi\cdot\sin(\psi) & -\lambda-\theta\cdot\sin(\psi)-\phi\cdot\cos(\psi) & 1 \end{bmatrix} \cdot \begin{bmatrix} 0 \\ -\sin(\alpha)\cdot\cos(\beta) \\ \sin(\alpha)\cdot\sin(\beta) \\ \cos(\alpha) \end{bmatrix}$$

Which can itself be condensed to:

$$\begin{bmatrix} 1 & 0 & 0 & 0 \\ 0 & 1 & A & B \\ 0 & -A & 1 & C \\ 0 & -B & -C & 1 \end{bmatrix} \cdot \begin{bmatrix} 0 \\ -\sin(\alpha)\cdot\cos(\beta) \\ \sin(\alpha)\cdot\sin(\beta) \\ \cos(\alpha) \end{bmatrix}$$

This expression can be used to find **(αnew,βnew)** to define the new boresight, as follows:

$$\begin{bmatrix} 0 \\ -\sin(\alpha new)\cdot\cos(\beta new) \\ \sin(\alpha new)\cdot\sin(\beta new) \\ \cos(\alpha new) \end{bmatrix} := \begin{bmatrix} 1 & 0 & 0 & 0 \\ 0 & 1 & A & B \\ 0 & -A & 1 & C \\ 0 & -B & -C & 1 \end{bmatrix} \cdot \begin{bmatrix} 0 \\ -\sin(\alpha)\cdot\cos(\beta) \\ \sin(\alpha)\cdot\sin(\beta) \\ \cos(\alpha) \end{bmatrix}$$

The approximate (but fairly accurate) solutions are found to be

$$\alpha new = \alpha + [\mu - \phi * \sin(\psi) + \theta * \cos(\psi)] * \cos(\beta) + (\lambda + \phi * \cos(\psi) + \theta * \sin(\psi) * \sin(\beta)) \qquad \textbf{(7-1)}$$

$$\beta new = \beta + [\nu + \delta] + \frac{[\lambda + \theta * \sin(\psi) + \phi * \cos(\psi)] * \cos(\alpha) - \sin(\beta) * (\alpha new - \alpha)}{\sin(\alpha new) * \cos(\beta)} \qquad \textbf{(7-2)}$$

Equations (7-1) and (7-2) indicate that **αnew-α** and **βnew-β** will tend to be maximised if **λ, μ, ν, θ, δ,** and **ϕ** have the same sign (except when **β**=0, the photometer case, in which case **ϕ** should have the opposite sign to the rest).

7.2. Effect on the boresight position on M3

Again, with all angular tilts being small, the full approximate expression for the transformation of the location of the point where the boresight vector meets M3 is given by (note Xf is used instead of XF, Yf instead of YF etc.)

$$\begin{bmatrix} 1 & 0 & 0 & 0 \\ 0 & 1 & 0 & 0 \\ 0 & 0 & 1 & \lambda \\ 0 & 0 & -\lambda & 1 \end{bmatrix} \cdot \begin{bmatrix} 1 & 0 & 0 & 0 \\ 0 & 1 & 0 & -\mu \\ 0 & 0 & 1 & 0 \\ 0 & \mu & 0 & 1 \end{bmatrix} \cdot \begin{bmatrix} 1 & 0 & 0 & 0 \\ 0 & 1 & \nu & 0 \\ 0 & -\nu & 1 & 0 \\ 0 & 0 & 0 & 1 \end{bmatrix} \cdot \begin{bmatrix} 1 & 0 & 0 & 0 \\ Xf & 1 & 0 & 0 \\ Yf & 0 & 1 & 0 \\ Zf & 0 & 0 & 1 \end{bmatrix} \cdot \begin{bmatrix} 1 & 0 & 0 & 0 \\ 0 & 1 & \delta & 0 \\ 0 & -\delta & 1 & 0 \\ 0 & 0 & 0 & 1 \end{bmatrix} \cdot \begin{bmatrix} 1 & 0 & 0 & 0 \\ 0 & \cos(\psi) & \sin(\psi) & 0 \\ 0 & -\sin(\psi) & \cos(\psi) & 0 \\ 0 & 0 & 0 & 1 \end{bmatrix} \cdot \begin{bmatrix} 1 & 0 & 0 & 0 \\ 0 & 1 & 0 & -\theta \\ 0 & 0 & 1 & 0 \\ 0 & \theta & 0 & 1 \end{bmatrix} \cdot \begin{bmatrix} 1 & 0 & 0 & 0 \\ 0 & 1 & 0 & 0 \\ 0 & 0 & 1 & \phi \\ 0 & 0 & -\phi & 1 \end{bmatrix} \cdot \begin{bmatrix} 1 & 0 & 0 & 0 \\ 0 & \cos(\psi) & -\sin(\psi) & 0 \\ 0 & \sin(\psi) & \cos(\psi) & 0 \\ 0 & 0 & 0 & 1 \end{bmatrix} \cdot \begin{bmatrix} 1 \\ Xm3-Xf \\ Ym3-Yf \\ Zm3-Zf \end{bmatrix}$$

Note that the 4-vector representation of the co-ordinates of a point allow the translations to be dealt with using a 4x4 matrix in the same way as the rotations. The difference is that the 4-vector for a point has unity in the first row, whereas the 4-vector representing a vector has zero in the first row. The above expression simplifies to

$$\begin{pmatrix} 1 \\ Xm3new \\ Ym3new \\ Zm3new \end{pmatrix} = \begin{pmatrix} 1 \\ Xm3 \\ Ym3 \\ Zm3 \end{pmatrix} + \Delta M3(Xm3, Ym3, Zm3, Xf, Yf, Zf, \psi, \theta, \phi, \delta, \lambda, \mu, \nu) \tag{7-3}$$

With

$$\Delta M3 = \begin{bmatrix} 0 \\ (\delta+\nu)\cdot Ym3 - \delta\cdot Yf + (\phi\cdot\sin(\psi) - \theta\cdot\cos(\psi) - \mu)\cdot Zm3 + (\theta\cdot\cos(\psi) - \phi\cdot\sin(\psi))\cdot Zf \\ -(\delta+\nu)\cdot Xm3 + \delta\cdot Xf + (\phi\cdot\cos(\psi) + \theta\cdot\sin(\psi) + \lambda)\cdot Zm3 - (\phi\cdot\cos(\psi) + \theta\cdot\sin(\psi))\cdot Zf \\ ((\theta\cdot\cos(\psi) - \phi\cdot\sin(\psi) + \mu)\cdot Xm3 + (\phi\cdot\sin(\psi) - \theta\cdot\cos(\psi))\cdot Xf) - ((\phi\cdot\cos(\psi) + \theta\cdot\sin(\psi)) + \lambda)\cdot Ym3 + (\phi\cdot\cos(\psi) + \theta\cdot\sin(\psi))\cdot Yf \end{bmatrix}$$

The additional effects of displacements (δXf, δYf, δZf) of the SPIRE reference point F1 (due to misplacement of the SPIRE box), and displacements (δXH, δYH, δZH) of the HOB from their respective nominal locations are included as follows:

$$\Delta M3TOT(\delta XH, \delta YH, \delta ZH, \delta Xf, \delta Yf, \delta Zf, \Delta M3) := \begin{bmatrix} 0 \\ \delta XH \\ \delta YH \\ \delta ZH \end{bmatrix} + \begin{bmatrix} 0 \\ \delta Xf \\ \delta Yf \\ \delta Zf \end{bmatrix} + \Delta M3 \tag{7-4}$$

The three contributions to the resultant displacements in each of the three axes should have the same sign in order to maximise their resultant sum. Equation (7-3), with ΔM3TOT from eq. (7-4) used instead of ΔM3, gives the new displaced co-ordinates of the actual point on M3 where the original SPIRE gut ray meets it. It has been moved because of all the tilts and decentres applied to SPIRE and the HOB. This point will be labelled PM3new. There is a corresponding 'new' boresight position, corresponding to the point where PM3new should be located, based on the 'new' boresight pointing angles **(αnew,βnew)**. This point will be labelled PBOREnew and its co-ordinates are derived as follows:

$$PBOREnew = \begin{pmatrix} XBOREnew \\ YBOREnew \\ Zborenew \end{pmatrix} = \begin{pmatrix} Zbore * \tan(\alpha new) * \sin(\beta new) \\ Zbore * \tan(\alpha new) * \cos(\beta new) \\ Ztot - Zbore \end{pmatrix}$$

Ztot and Zbore are shown in figure 4-1. Figure 7-1 shows the relationship between these two points and the origin as might occur using representative values for all the tilts and displacements. The figure illustrates how the lateral offsets and the effective defocus are computed:

$$\begin{pmatrix} Xoff \\ Yoff \\ defocus \end{pmatrix} = \begin{pmatrix} R * \cos(W - \beta new) - Rbore \\ R * \sin(W - \beta new) \\ Xoff * \sin(\alpha new) - \Delta Zm3 * \cos(\alpha new) \end{pmatrix} \tag{7-5}$$

The convention adopted for the defocus is that a POSITIVE defocus INCREASES the distance of M3 from M2 along the gut ray. The above expression is correct for both positive and negative values for both Xoff and ΔZm3. Figure 7-1 illustrates a situation where defocus is negative, Xoff is negative, Yoff is positive and ΔZm3 will have a negative sign. In figure 7-1, R and Rbore are the radial distances from the origin of co-ordinates of the projections of the points PM3new and PBOREnew onto the plane containing PBOREnew. They are computed from the X and Y co-ordinates of PBOREnew and PM3new. The angle W can also be computed using the X and Y co-ordinates of PM3new. See table 7-1 for the formulae.

Table 7-1 Formulae for R, Rbore and W

quantity	Derivation in terms of given quantities
R	$\sqrt{Xm3new^2 + Ym3new^2}$
Rbore	$\sqrt{XBOREnew^2 + YBOREnew^2}$
W	$\sin^{-1}(Ym3new/R)$

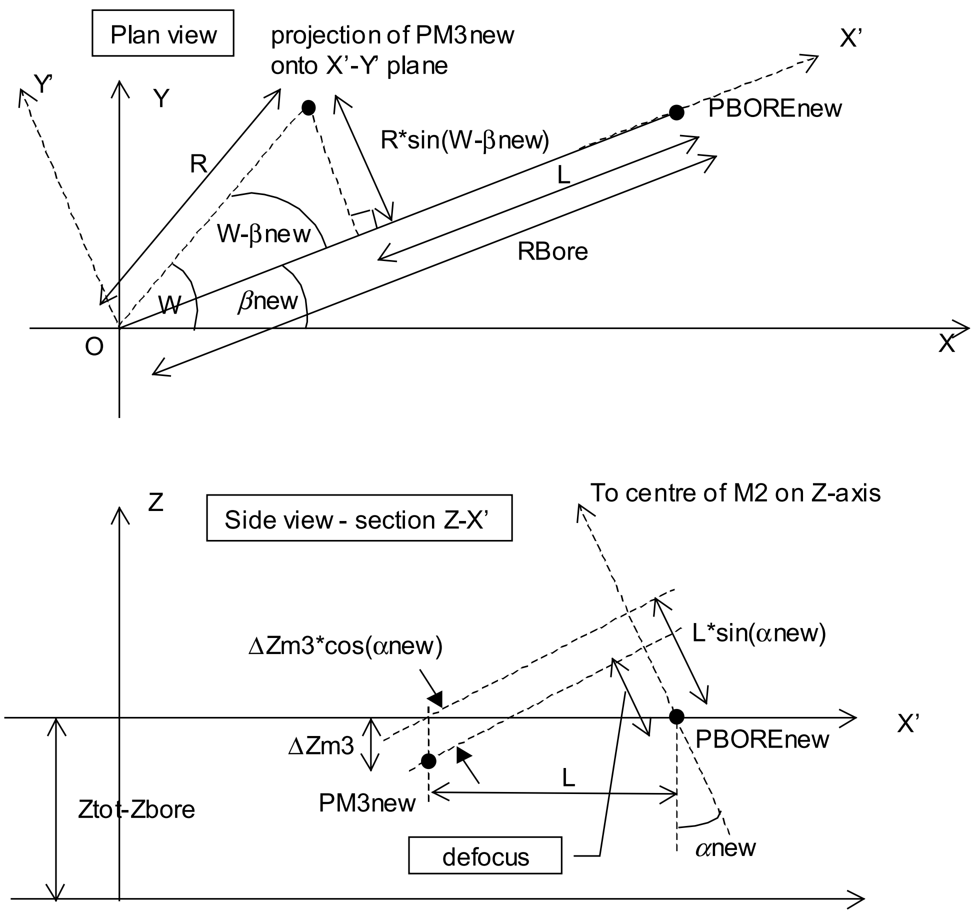

Figure 7-1 Derivation of lateral offsets and defocus relative to 'new' boresight position for M3

8. SAMPLE COMPUTATIONS

Table (8-1) summarises the data used for modelling the movement of each instrument. The co-ordinates of the boresight (gut ray) vector on M3 for each instrument were used to determine the (α,β) angles that define each gut-ray direction.

Table 8-1 Modelling data

Quantity	Definition/value	Photometer	Spectrometer
Zfoc	Distance M2→axial focus	2638	2638
Ztot	Distance M2→Optical bench reference surface = Zfoc+202	2840	2840
Xm3	Gut-ray intersection point on M3, X co-ordinate, wrt optical bench	93.49323	93.34246
Ym3	Gut-ray intersection point on M3, Y co-ordinate, wrt optical bench	0.0	-62.76123
Zm3	Gut-ray intersection point on M3, Z co-ordinate, wrt optical bench	131.14159	136.53084
Zbore	Distance M2→ plane containing gut ray intersection = Ztot-Zm3	2708.85841	2703.46916
α	Bore sight angle to Z-axis = $\tan^{-1}\left[\sqrt{Xm3^2 + Ym3^2} / Zbore\right]$	1.9767 deg.	2.38247 deg.
β	Azimuth of plane containing boresight vector = $\tan^{-1}\left[Ym3/Xm3\right]$	0.0 deg	-33.916 deg
Xf	Reference foot X-co-ordinate	0	0
Yf	Reference foot Y-co-ordinate	0	0
Zf	Reference foot Z-co-ordinate	30	30
ψ	Angle of line from fixed foot to outer foot to fold plane	30 deg	30 deg
q	Basic unit of angular tilt, radians	0.0003	0.0003
θ, φ, δ	Tilts of SPIRE box on the HOB, radians	q, -q, q	q, -q, q
λ, μ, ν	Tilts of the HOB, radians	q, q, q	q, q, q
δc	Unit of displacement, mm	0.5	0.5
δXf, δYf, δZf	Displacements of the SPIRE box on the HOB	-δc, -δc, δc	-δc, -δc, δc
δXH,δYH,δZH	Displacements of the HOB relative to the telescope	-δc, -δc, δc	-δc, -δc, δc

As a preliminary to a more detailed study, boresight changes, offsets and defocus values have been computed with the magnitude of all tilts set to 1 arc minute, which equals approximately 0.0003 radians. The signs were chosen to maximise their effects. Also, the angle ψ was assumed = 30 degrees. The displacements (δXf,δYf, δZf) of the SPIRE reference point F1, and the displacements (δXH,δYH, δZH) of the HOB were all given magnitude =0.5 mm and their signs were also matched to maximise their total effect by observing the results. Typical results were as follows (results in mm):

Table 8-2 Typical results of computations

Quantity	Photometer	Spectrometer
Xoff	-1.58	-1.72
Yoff	-3.03	-3.02
Defocus	-1.16	-1.14
$\sqrt{Xoff^2 + Yoff^2}$	3.41	3.48
αnew-α	0.0407	0.028 deg
βnew-β	0.343	0.788 deg

The root-sum-squared (RSSQ) of Xoff and Yoff is the magnitude of the resultant lateral movement of the instrument's gut ray away from the centre of M2. This is also the magnitude of the resultant lateral movement of the image of the instrument pupil projected out to M2, since its reference is the gut ray projected out from SPIRE. It was found that the shifts of the M3 location due just to the 1 arc-minute tilt misalignments, given by ΔM3, were much smaller than the typical 1 mm shifts applied to the HOB and the SPIRE reference point due to the addition of the separate HOB and SPIRE lateral shifts (see eq. 7-3 and eq. 7-4).

Typical changes to the boresight elevation angle α, measured from the telescope axis of symmetry, were found to be about 0.04 degrees, or 2.4 arc minutes. When the telescope magnification factor of about 10 is taken into account, this equates to a change in boresight angle on the sky of about $1/10^{th}$ this value.

It is possible to decide on a maximum value we want to permit α to change by, and use equation 7-1 to derive limits for the angles λ,θ and ϕ. That equation can also be used to determine a RMS value for the change in α, given RMS values for the three angles concerned (assuming that the tilts add in quadrature i.e. they are each drawn at random from normal-like populations with well-defined mean values). With all the equations programmed in Mathcad, it is straightforward to determine typical pupil shifts and boresight changes given various magnitudes for the tilt and lateral offsets.

9. FURTHER WORK

The sample computations take uniform tilts and uniform displacement magnitudes and sum their effect to give a resultant misalignment that should be near the worst case. However, not all the tilts and/or displacements will add in general, if the residual misalignments are in practice uncorrelated and random in nature.

One possible way forward is to assume that the tilts will be uncorrelated and random and to devise 3-sigma values which would give pupil shifts and boresight angular changes within a specified limiting range for a fraction of cases equal to the integral between 3-sigma points on each assumed distribution. This will require some Monte Carlo calculations of the quantities derived in the above notes, given random choices of the independent variables from selected uniform distributions.

10. MONTE CARLO CALCULATIONS

10.1. Determination of the distributions of random boresight displacements and tilts

Extensive Monte Carlo computations have now been carried out to try and determine formulae which can predict 3-sigma boresight displacement and boresight alignment changes resulting from random tilts and displacements of SPIRE. In order to do this, the six tilts and six displacements listed in table 8-1 were replaced with quantities derived from numbers randomly drawn from a uniform distribution over the range –1.0 to +1.0 having zero mean. A random number was multiplied by either the basic tilt unit (0.0003 radians, 1 arc minute) or the basic displacement unit (0.5 mm) to get a tilt or displacement value, respectively. That is, the angular tilt of each axis was randomly chosen to be in the range –1 arc minute to +1 arc minute and the lateral displacement in each axis was randomly chosen to be in the range -0.5 mm to +0.5 mm. The 'random values were then used in the equations to derive values for the six quantities listed in table 8-2. This was repeated 1000 times to get 1000 values for each of the six quantities. As the following figures confirm, the root-sum-squared (RSSQ) boresight displacements, angular tilt and defocus can all be approximated by normal (Gaussian) distributions. Their means and standard deviations (σ) were obtained and values for (mean+3σ) determined. Some results are shown in the following tables and figures.

	Photometer			Spectrometer		
quantity	mean	**σ**	Mean+3**σ**	mean	**σ**	Mean+3**σ**
$\sqrt{Xoff^2 + Yoff^2}$	1.67	0.874	4.29	1.66	0.875	4.29
αnew-α (deg)	0.0013	0.025	0.075	0.009	0.024	0.073

Table 10-1 Typical statistics for boresight displacement and tilt

Based on the RSSQ offset of the boresight being the result of 4 lateral displacements (X and Y displacements of the HOB and of SPIRE on the HOB) of mean value 0.5 mm plus 4 tilts causing lateral displacement of the boresight at M2 (at a distance 2840 mm) of mean value 2840*tan(1 arc minute)=0.826 mm, we would expect a RSSQ of all 8 effects to be $\sqrt{4*0.5^2 + 4*0.826^2} = 1.93$, compared to the value 1.67 obtained statistically. The mean+3σ values typically cover 0.998 of the population in a normal distribution of the given mean and standard deviation.

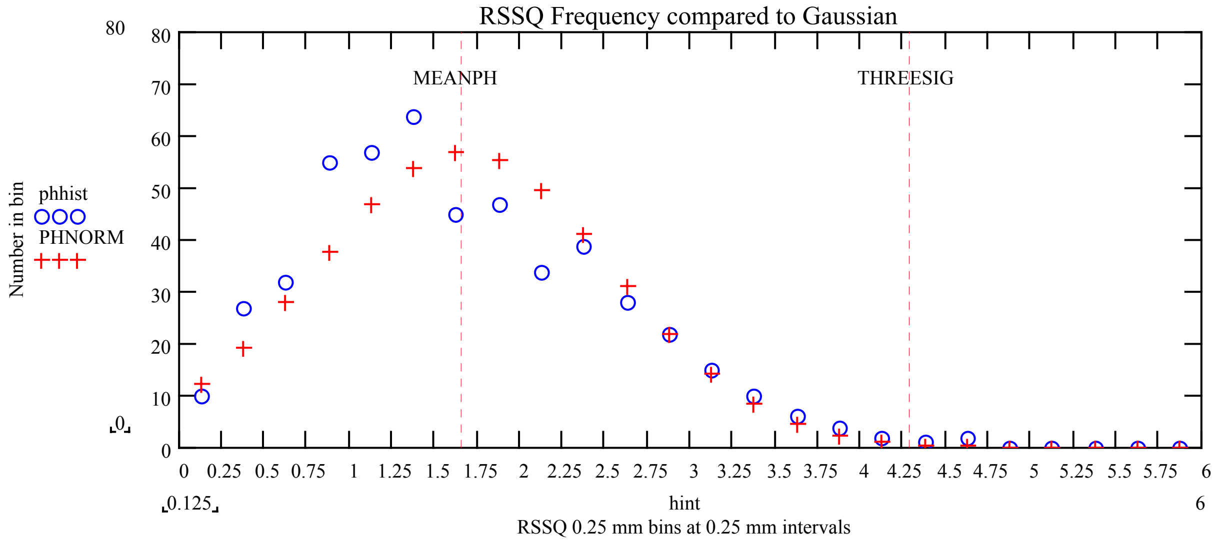

Figure 10-1 Circle = Statistics of the computed Photometer RSSQ displacement of boresight. Crosses are expected frequencies for a normal distribution having the same mean and standard deviation as the sample population.

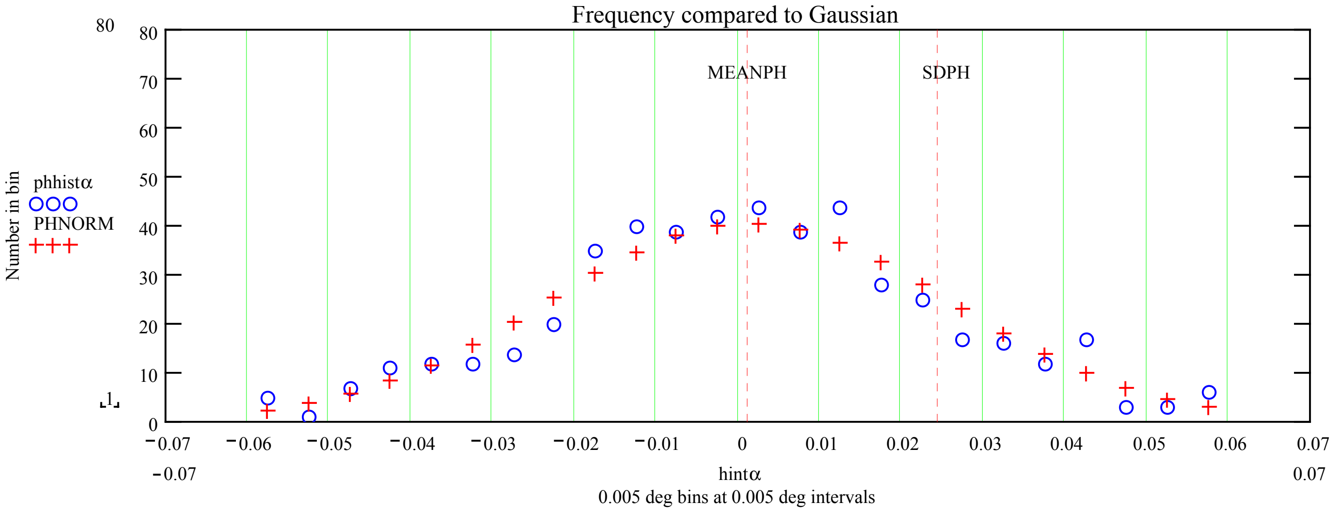

Figure 10-2 Statistics of the computed Photometer displacement of boresight elevation angle. Crosses are expected frequencies for a normal distribution having the same mean and standard deviation as the sample population.

10.2. Determination of formulae for predicting 3-σ boresight displacements, tilts and defocus.

The preceding section showed that the boresight displacements and tilts etc. follow normal distributions, given random tilts and displacements of SPIRE. What is ultimately desired is the ability to specify the maximum permitted ranges or amplitudes of these random tilts and displacements of SPIRE so as to ensure that 3-σ values for the boresight displacement and tilt remain within a budgeted limit. In order to do this, we need to determine the general relationship between the SPIRE random tilt and displacement amplitudes and the expected 3-σ values for the boresight parameters that result.

Let the tilt noise amplitude Q in units of q (with q= 1 arc minute) be denoted by

$$Q(m) = m * q \qquad \textbf{(10-1)}$$

and let the displacement noise amplitude Δ in units of δ (with δ=0.5 mm) be denoted by

$$\Delta(n) = n * \delta \qquad \textbf{(10-2)}$$

This means that tilts are to be randomly drawn with equal probability between –Q(m) and +Q(m) arc minutes and displacements are to be randomly drawn with equal probability between –Δ(n) and +Δ(n) mm. The resulting distributions of boresight tilts and pupil misalignments can then be labelled with the number pair (m, n). Since the numbers m and n can independently take on any positive values from 0 upwards, there is a double infinity of possible pairs to be covered. Taken together, (m, n) maps the whole positive quadrant of the 2-dimensional plane and the computations done so far are for the single point (1,1) in that plane (see figure 10-3). All points that maintain the same ratio of n/m lie on the same line through the origin that makes an angle $\theta = \tan^{-1}(n/m)$ with the horizontal axis, so points (1.1), (1.52,1.52) and similar points lie on a line at 45 degrees. All such points describe cases where the amplitudes of the random angular tilts and lateral displacements of SPIRE have the same constant ratio q/δ. A general point (m,n) describes cases where the angular tilt and lateral displacement amplitudes have the same constant ratio $m*q/n*\delta$. What we are looking for is some general method of choosing a pair of values for (m, n) that will result in a particular 3-σ value for the RSSQ displacement say, or the 3-σ value for the boresight elevation angle change.

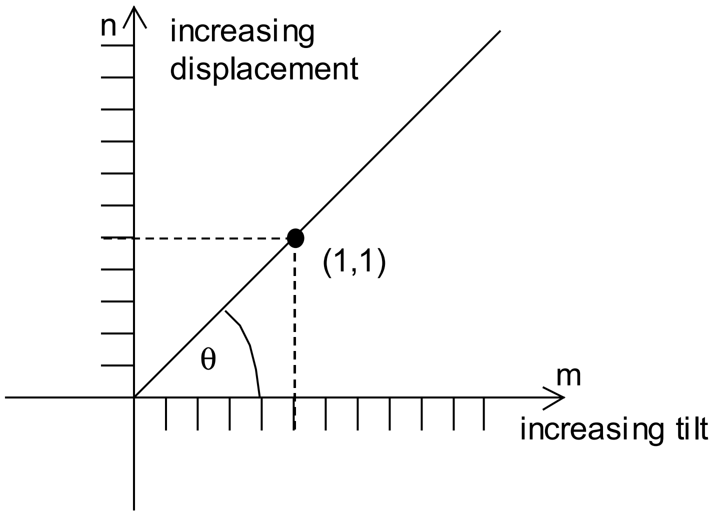

Figure 10-3 The domain of random tilts and displacements in terms of real numbers m and n

A further series of Monte Carlo computations were carried out for distributions covered by the following (m,n) pairs: (2,2), (3,3), (4,4), (5,5). These gave points on the line drawn in figure 10-3 making an angle θ=45 degrees to the horizontal axis. It was found that the 3-σ values that resulted were proportional to the distance $R(m,n) = \sqrt{m^2 + n^2}$ along the line from the origin passing through the points. Further computations showed that other (m,n) pairs along other radial lines scaled similarly and the scale factor varied with the angle θ. The results of the computations are summed up in figures 10-4, 10-5 and 10-6, which show plots of 3-σ values for the RSSQ pupil displacements, the boresight elevation tilt and the defocus shift, each divided by R(m,n) and plotted as a function of $\theta(m,n) = \tan^{-1}\{n/m\}$. The scatter at each θ-value is due to statistical noise. The apparent sinusoidal relationship between the 3-σ values and the angle θ is confirmed by the curves drawn through the points. These curves represent the relationships expressed in equations (10-3), (10-4) and (10-5). In each case, no attempt has been made to optimise the fitted curve.

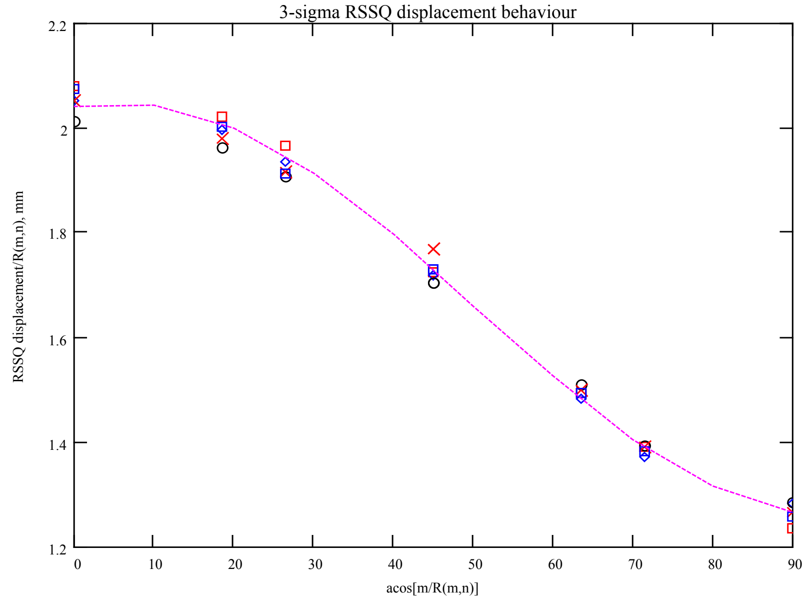

Figure 10-4 RSSQ 3-σ/R(m,n)

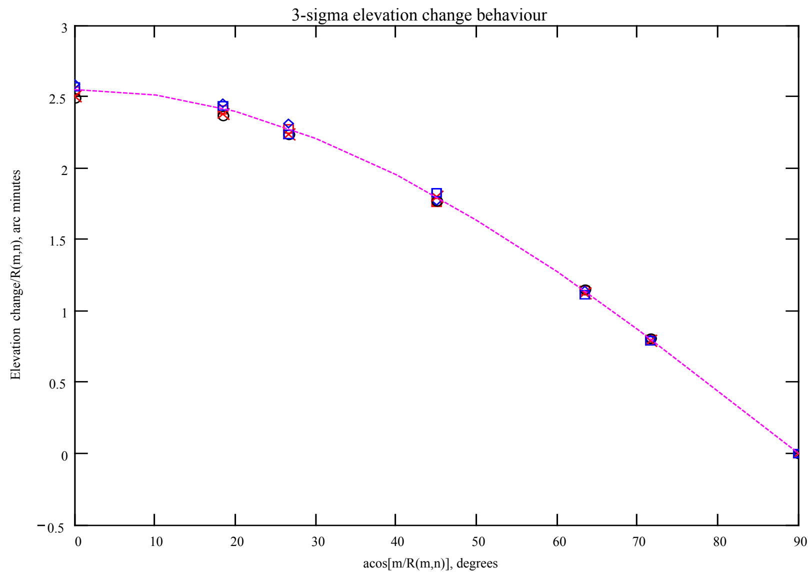

Figure 10-5 3-σ Elevation changes/R(m,n)

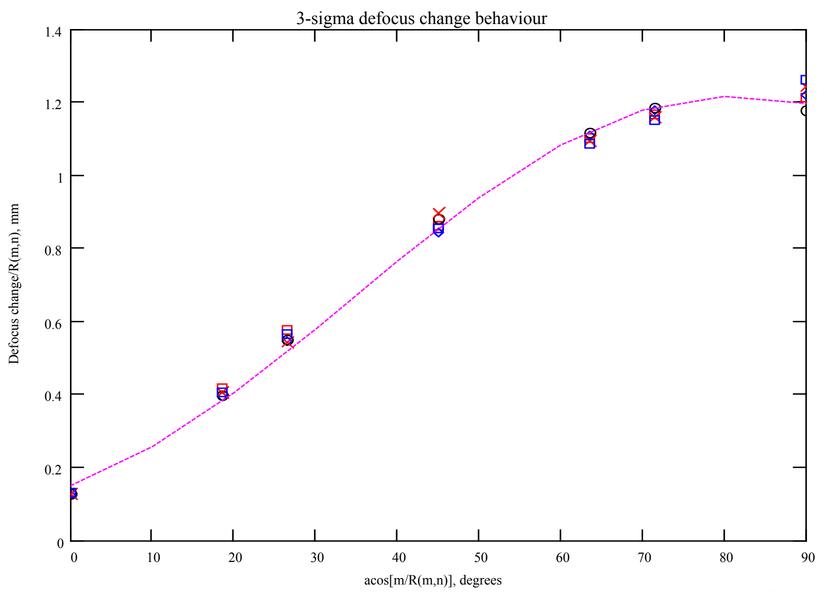

Figure 10-6 3-σ defocus changes/R(m,n)

$$RSSQ(m,n) = R(m,n) * \{1.655 + 0.395 * \cos(2\theta - 11)\}$$ **(10-3)**

$$\delta\alpha(m,n) = R(m,n) * 2.55 * \cos(\theta)$$ **(10-4)**

$$\delta focus(m,n) = R(m,n) * \{0.66 + 0.56 * \sin\{1.9\theta - 65\}$$ **(10-5)**

$$R(m,n) = \sqrt{m^2 + n^2}$$ **(10-6)**

$$\theta(m,n) = \tan^{-1}\{n/m\}$$ **(10-7)**

Equations (10-3) and (10-5) gives displacements in millimetres, equation (10-4) gives $\delta\alpha$ in arc minutes.

11. TILT AND DISPLACEMENT BUDGETS FOR GIVEN MAXIMUM RSSQ PUPIL DISPLACEMENT.

The above equations sum up the results of the Monte Carlo modelling. Equation (10-7) shows that θ decreases with m, and increases with n. Larger values of θ denote smaller multiples (m) of tilt amplitudes compared to multiples (n) of displacement amplitudes and smaller values of θ denote larger tilt multiples (m) compared to displacements (n).

It is clear from the figures that the largest RSSQ displacements and boresight tilts are given at smaller values of θ, around θ=11/2 degrees, whereas the defocus effects are maximised at the other end of the scale, near θ= 77 degrees. If we consider a particular case where we wish the 3-σ RSSQ boresight displacement at M2 to be 9 mm, or about 6% of the pupil (M2) radius, then we must use the inverse of equation (10-3) to determine values for R(m,n) and, ultimately, m and n that will give RSSQ=9 millimetres.

We start by **choosing** θ=11/2 degrees, so that the angular factor is maximised to = 2.05 and the ratio n/m=tan(11/2). This will **minimise** the permitted value for R(m,n). From equation (10-6) it follows that R(m,n)=m/cos(11/2) and inversion of equation (10-3) gives R(m,n)=9/2.05, from which it follows that m=9*cos(11/2)/2.05=4.37 and hence n=m*tan(11/2)=0.42. These values for m and n can then be used in equations (10-1) and (10-2) to get random tilt and displacement amplitudes.

The conclusion is that for a 3-σ RSSQ boresight displacement at M2 = 9 mm, the allowed random tilt amplitudes can be up to +or- 4.37 arc minutes and the allowed random displacements can be up to +or – 0.42*0.5=0.21 mm. As the above calculations show, by choosing a different value for θ, the angular factor will be smaller, leading to a larger permitted value for R(m,n). This will in general permit larger values for one or both of m and n and hence larger random tilt and displacement amplitudes. However, the relationships involving R(m,n) show that a correlation exists between the permitted values for m and n for a given RSSQ value sought. Therefore it follows that if one chooses a maximum random tilt amplitude, the maximum random displacement amplitude must be derived from the equations using the maximum allowed 3-σ RSSQ boresight displacement. Alternatively, it follows that if one chooses a maximum random displacement amplitude, the maximum random tilt amplitude must be derived from the equations using the maximum allowed 3-σ RSSQ boresight displacement.

For example, suppose we wish to relax the random displacement amplitude by a factor 10, from the above computed minimum of + or - 0.21 mm to + or – 2.1 mm. What are the consequences for the allowed random tilt amplitudes? The new random displacement limit requires n=10*0.42=4.2. This in turn means m=4.2/tan(θ) and R(m,n)=4.2/sin(θ). We therefore have to solve the following equation for θ:

$$9 = \frac{4.2}{\sin(\theta)}\left\{1.655 + 0.395\cos(2\theta - 11)\right\} \qquad \textbf{(11-1)}$$

MathCad gives the solution θ=50.54 degrees, giving m=4.2/tan(θ)=3.46. Therefore the permitted random tilt amplitudes must be reduced to 3.46 arc minutes from the earlier 4.37 arc minutes. Thus a factor 10 increase in the permitted random displacement amplitude, to 2.1 mm, necessitates only a factor 0.8 reduction in the permitted random tilt amplitude. In this fashion, trade-offs can be made between random tilt and random displacement amplitudes. If the 3-σ RSSQ displacement is regarded as the driving factor, then equation (10-3) links all the variables and equations (10-4) and (10-5) can then be used to derive likely 3-σ boresight tilts and 3-σ defocus shifts resulting from the solution of equation (10-3) for the variables m, n and θ. The 3-σ boresight elevation tilt δα= 8.82 arc minutes corresponding to the θ=50.54 degree solution. The corresponding 3-σ defocus shift = 5.16 mm.

12. CONCLUSIONS

General relationships have been established that enable the determination of permitted angular tilts and co-ordinate shifts that will keep 3-σ boresight displacements below a permitted budget limit of 9 millimetres. **Typical permitted random tilt amplitudes are around 3.5 arc minutes per axis** and **corresponding displacement amplitudes may be as high as 2.1 millimetres per axis**. Defocus 3-σ values would then be as high as 5.16 millimetres and 3-σ boresight elevation tilts as high as 8.82 arc minutes. The 3.5 arc minutes tilt amplitudes can be used to specify a flatness criterion for the HOB surface to which SPIRE interfaces, so that the tilts shown in figure (5-1) as being due to mounting feet displacements remain below the quoted size. This turns out to be 1 millimetre in 1000 mm. This is quite a relaxed tolerance.

Because of the correlated effects of the two main sources of boresight displacements (SPIRE tilts and shifts), setting a certain permitted level of 'noise' in one of them simultaneously constrains the other source of noise to remain within certain limits, given a certain budgeted 3-σ value for the permitted boresight displacement. Other constraints that ought to be considered are a possible maximum permitted defocus shift and maximum permitted boresight elevation tilt. The defocus constraint in particular will tend to shift the θ-solutions to lower values, as figure (10-6) shows, whereas lower θ-values tend to increase the 3-σ RSSQ values, as figure (10-4) shows.

If it is impossible to meet the requirements on limiting the amplitudes of one or both random sources of boresight displacement to values quoted above, one possibility is to relax the requirements by specifying 2-σ values instead of 3-σ values. By itself this will permit an increase in the noise amplitudes by a factor of about 3/2. This is because the 2-σ values are a factor 1.5 smaller than the of 3-σ values (at least for quantities with zero mean, so that the ratio of (mean+3σ) values to (mean+2σ) values = 3/2 applies), so to reach a given boresight displacement will require increasing the noise amplitudes by the same factor. A further increase in noise amplitudes is available if 1-σ values are specified. Table (12-1) below shows the probability of each of these values being exceeded given a normal Gaussian distribution of values with given mean μ and standard deviation σ.

Table 12-1 Gaussian probabilities

Value	Probability of obtaining a value less than the quoted value by chance	Probability of obtaining a value greater than the quoted value by chance
μ+σ	0.8414	0.1586
μ+2σ	0.97723	0.02277
μ+3σ	0.99865	0.00135

Thus whereas there is only a 0.135% chance of obtaining a value exceeding μ+3σ, there is a 2.277% chance of obtaining a value exceeding μ+2σ, and a significant 15.86% chance of obtaining a value greater than μ+σ. So, if we accept the small increase in probability that a μ+2σ threshold gives us, we could accept increased random tilt amplitudes of 1.5*3.5=5.25 arc minutes and random displacement amplitudes of 1.5*2.1=3.15 millimetres.

Another possible way of increasing permitted tilt and displacement amplitudes is to treat the 3 axes differently. That is, it might be possible to apply tighter limits to one or more axes because of the ability to ensure more accurate placement in that axis. These axes will then make a smaller contribution to the overall budget, releasing the balance to be distributed between the other axes, permitting larger amplitudes for them. However it is not possible, with the information presently available, to identify which, if any, axes are likely candidates for this treatment. Nevertheless, if needed, it is theoretically feasible to extend the present modelling technique, where all axes are treated identically, to introduce weighting factors which assign different tilt or displacement amplitudes to each axis.